Rational Design for the Controlled Aggregation of Gold Nanorods *via* Phospholipid Encapsulation for Enhanced Raman Scattering

Alexander F. Stewart,[†] Anna Lee,[‡] Aftab Ahmed,[§] Shell Ip,[†] Eugenia Kumacheva,[†] and Gilbert C. Walker[†,*]

[†]Department of Chemistry, University of Toronto, Toronto, Ontario M5S3H6, Canada, [‡]Department of Electrical and Computer Engineering, University of Toronto, Toronto, Ontario M5S3G4, Canada, and [§]Department of Electrical and Computer Engineering, University of Waterloo, Waterloo, Ontario N2L3G1, Canada

ABSTRACT This study describes a procedure that found a balance between the ability of polymer-stabilized nanorods (NRs) to self-assemble and the creation of narrow gaps to make reproducibly bright surface-enhanced Raman scattering (SERS) nanorod dimers. NRs were end-functionalized with polymers, which enabled end-to-end self-assembly of NR chains and control over inter-rod separation through polymer molecular weight (MW). We found a way to quench the self-assembly, by phospholipid encapsulation, reducing the polydispersity of the aggregates while rendering them water-soluble. This reduction in polydispersity and preferential isolation of short-chain nanorod species is important for maximizing SERS enhancement from nanorod chains. We prepared NR aggregates that exhibit ~5−50 times greater SERS intensity than isolated rods (and ~750× greater than bare dye) depending on inter-rod separation, when using Oxazine 725 reporter molecules. Colloidal stability of NR aggregates and temporal stability of the SERS signal in water were observed for 110 days. With enhanced SERS intensity, water solubility, and stability, these NR aggregates are promising optical probes for future biological applications.

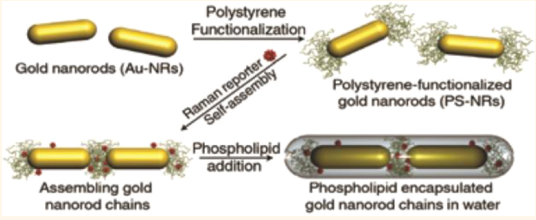

KEYWORDS: nanorods · self-assembly · lipid encapsulation · SERS probes · biodiagnostic probes

Interactions between localized surface plasmon resonances (LSPRs) of adjacent metal nanoparticles (NPs) enable energy concentration and transport for applications in sensors and medical diagnostics.[1−4] Bright surface-enhanced Raman scattering (SERS) probes have been made by multiple approaches.[5] The state of the art is represented by core−shell structures or nanoparticle aggregates.[6] Recently, assembly of NP aggregates has been achieved *via* electrostatic interactions,[7] coordination chemistry,[8] and hydrophobic forces.[9] Lack of control of the particle−particle aggregate structures leads to great variation in SERS intensity.[10] This is because the LSPRs of the NPs are affected by particle proximity, as well as their orientation and extent of aggregation.[11] High-purity isolation of self-assembled spherical NP dimers has been achieved, but these methods require multiple purification steps involving harsh centrifugation conditions,[12] and isolation was not achieved for nanorod-based species.

End-functionalization of gold nanorods (NRs) to form end-to-end chains is a rational alternative that could provide uniform self-assembly, inter-rod gap control, and near-IR optical function.[13] To form such chains, NRs have been previously end-functionalized with associating ligands such as poly(vinylpyrrolidone)[14] or polystyrene.[13] Examinations of gold−silver core−shell nanorods for SERS enhancement have also been made.[15,16] Previous work[13,17] demonstrated the potential viability of self-assembled gold NR chains as SERS probes as a result of electric field "hotspots" that exist in the inter-rod gaps between illuminated, longitudinally assembled chains. However, previous work did not establish a method to form the NR oligomers that are small, bright, and stable enough for biodiagnostic applications. Long chains would not be effective for targeting proteins on cell surfaces, for example, as a result of both steric issues and the reduction of optical brightness in long chains (chains consisting of 4+ NRs).[13]

* Address correspondence to gwalker@chem.utoronto.ca; ekumache@chem.utoronto.ca.

Received for review August 26, 2013 and accepted May 14, 2014.

Published online May 14, 2014
10.1021/nn4044589

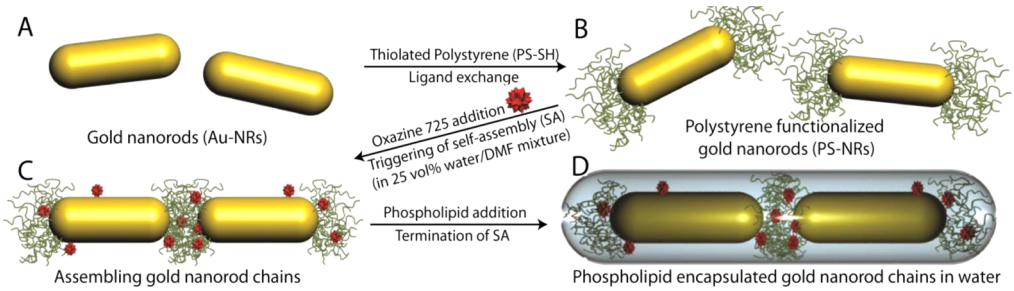

Scheme 1. Generation of lipid-encapsulated NR chains. (A) CTAB-stabilized gold NRs. (B) Thiolated polystyrene at the ends of gold NRs was introduced *via* a ligand exchange process. (C) Inclusion of Raman reporter (Oxazine 725) to the NR solution in DMF, followed by the self-assembly initiated *via* addition of water to 25 vol %. (D) Quenching of self-assembly *via* introduction of DEC221 phospholipid solution, encapsulating the self-assembling gold NR chains.

Control of the aggregation number is a challenge due to the progression of NR self-assembly.[13] An additional important challenge is to enable long-term colloidal stability in water, as well as a platform for immunotargeting.[18] A rational design for such probes is needed.

In the method reported here, we present a comprehensive approach to the generation of bright NR chain-based SERS probes. We describe the control of the inter-rod gap distance in the NR chains through the use of polymer linkers of steadily decreasing MW, strongly enhancing the signals of Raman reporters. We report a novel method of selective termination of nanorod assembly through phospholipid encapsulation of the self-assembling chains (previously shown effective on isolated NP species).[19−21] This results in control over the populations of the resultant nanorod chain structures (dimers/trimers, *etc*), for which no current reliable method exists. Finally, we demonstrate how this encapsulation (with an appropriate phospholipid that has been shown to support functionalization with biomolecules)[22] renders the resultant species water-soluble and stable over months, key requirements for any potential uses related to immunotargeting. Scheme 1 illustrates our approach.

RESULTS AND DISCUSSION

Synthesis, Assembly, and Encapsulation of Nanorods. Gold NRs were synthesized according to an established method[23] and tethered with thiolated polystyrene at both ends *via* ligand exchange (Scheme 1A/B).[24] Oxazine 725 as a Raman reporter was then introduced. Hydrophobicity-driven, end-to-end self-assembly of NRs was triggered by adding water to the solution of NRs in dimethylformamide (DMF, Scheme 1C). The gap between NR ends in the chains was controlled by selecting the MW of the end-tethered polystyrene molecules. Encapsulation of NR assemblies with phospholipids during the early self-assembly stages entrapped dimers and trimers of NRs (Scheme 1D).

Theoretical electric field modeling confirmed that the control of both the inter-rod gap size and the relative proportions of short-chain species is crucial in achieving maximized local electric field intensity. We found that reduction of an inter-rod gap size of ~9 nm (commonly achieved when utilizing 12 kDa polystyrene as a linking agent)[13] to ~2 nm would result in a significant increase in local field intensity, though within a reduced volume of the hotspot region (Supporting Information). Determination of the correct MW of polystyrene required for this reduced gap was therefore made. Isolation of large numbers of dimers and trimers would likewise result in an overall higher average solution field intensity (Supporting Information).

The NRs had the average length and diameter of 34.4 ± 6.4 and 7.5 ± 2.0 nm, respectively (determined *via* TEM). The molecular weights of the thiolated polystyrene were between 12, 5 and 2 kDa. The phospholipid used for NR encapsulation was DEC221, a mixture of 1,2-dioleoyl-*sn*-glycero-3-phosphocholine, egg sphingomyelin, and bovine cholesterol in a 2:2:1 molar ratio. The self-assembly progression was monitored by following the red-shift of the longitudinal LSPR extinction peaks of the NRs.[13] Figure 1A shows a typical evolution of extinction spectra of the NRs undergoing end-to-end self-assembly.

With increasing self-assembly time the longitudinal LSPR red-shifted, indicating that the average number of NRs per chain increased.[13] The inset shows extinction spectra of the NRs without encapsulation 15 s and 30 min after the beginning of self-assembly. Figure 1B shows that the lipid-encapsulated NR chains exhibited no further red-shift of the longitudinal LSPRs. This indicated the success of halting further NR chain growth.

Phospholipids were introduced 30 min after triggering the self-assembly. Termination of NR self-assembly occurred as a result of the formation of the lipid layer around NR chains. Population analysis was conducted *via* transmission electron microscopy (TEM) characterization of NR aggregates (exemplary images of NR chains are shown in Figure 2A). We note that the encapsulation of the NR aggregates within a lipid shell did not noticeably affect the mutual orientation of the NRs.[13] The optimal duration of self-assembly prior to encapsulation leading to the largest number of dimers and trimers was determined to be 30 min.

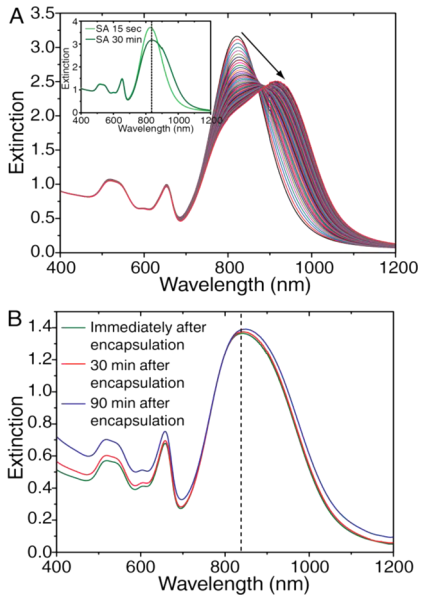

Figure 1. (A) Extinction spectra showing the red-shift of the longitudinal LSPR and peak broadening when self-assembly continues over 120 min. Inset: Snapshot of self-assembly progress at favorable encapsulation time. Transverse LSPR is observed at ~520 nm, and Oxazine 725 reporter is observed at 653 nm. (B) Extinction spectra acquired 0, 30, and 90 min after encapsulation (30, 60, and 120 min after initiation of self-assembly). Dotted line indicates peak position at the time of lipid introduction. The small observed increase in the transverse plasmon peak following encapsulation was attributed to broad background scattering loss from excess aggregating phospholipids, by comparison with phospholipid solutions lacking the nanorods (data not shown).

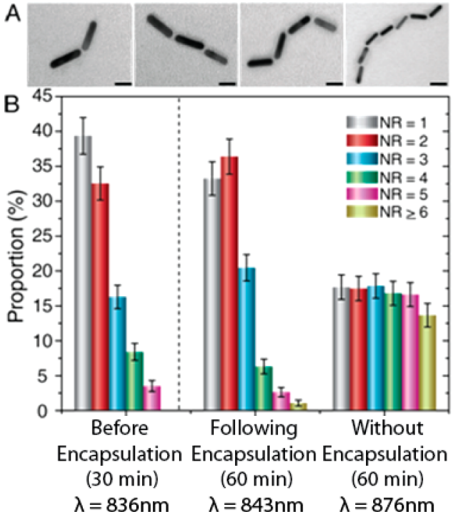

Figure 2. (A) Representative TEM images of encapsulated chains. The scale bars are 20 nm long in the first three images and 35 nm in the fourth image. The phospholipid layer is visible as a faint corona around the NR chains. (B) Fractions of various NR species at various stages of self-assembly and encapsulation, detailing the maximized short-chain proportions following encapsulation.

Figure 2B shows histograms corresponding to various stages of NR self-assembly both before and after encapsulation.

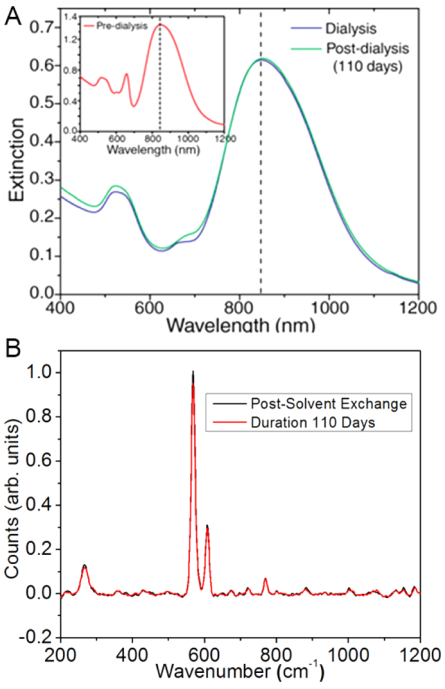

Figure 3. (A) UV–vis–NIR spectrum of an encapsulated NR solution immediately after solvent exchange and after 110 days, showing minimal deviation. (B) Raman spectra of the same solution showing minimal deviation in observed initial intensity and after 110 days.

Nanoprobe Stability over Time. Substantial numbers of monomers, dimers, and trimers with small numbers of longer chains were observed 30 min after the initiation of self-assembly (Figure 2B, left). Thirty minutes after encapsulation (total elapsed time = 60 min), a large fraction of short species was preserved (Figure 2B, middle). Importantly, when phospholipids were used for the encapsulation, the number of longer NR species remained constant. In contrast, without encapsulation at the same total elapsed time of 60 min (Figure 2B, right), the fraction of longer species was significantly increased at the expense of shorter species, in agreement with a step-growth polymerization process.[24] In order to produce water-stable NR-based lipid-encapsulated SERS probes, the resultant solution of short-chain species was subjected to solvent exchange *via* dialysis to replace the DMF with water. The removal of DMF was confirmed *via* both UV–vis–NIR (Figure 3A) and Raman spectroscopy (Figure 3B) of the encapsulated solution, and it was found that the nanoprobes were stable for an extended period of time in water (110 days). This is shown in Figure 3A and B.

Previous work shows an overall negative electrokinetic potential (ζ-potential) for NRs at the relative DMF/water amounts used here, consistent with the partial desorption of cetyltrimethylammonium (CTA) chains on the NR surface.[25]

Enhancement Efficiency with Differing Inter-rod Gap Lengths. Following dialysis, the ~0.13 nM (an estimate that was reached by applying molar extinction coefficients from

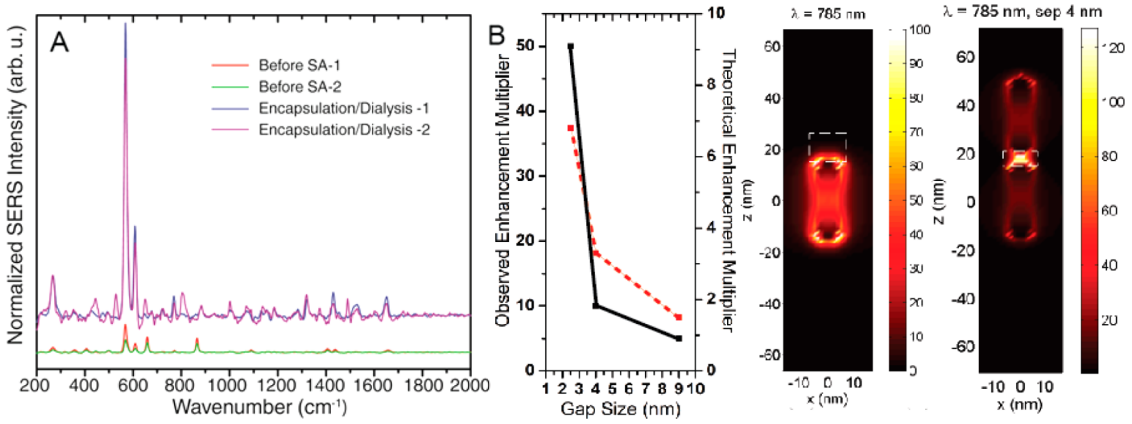

Figure 4. (A) Raman spectra of gold NR solutions utilizing a 5 kDa PS linker prior to (bottom) and following (top) NR self-assembly, encapsulation, and dialysis, corrected for NR concentration. (B) Comparison of predicted (red, dashed) and observed (black, solid) enhancement (assuming a dimeric solution and using theoretically predicted values of the square of the electric field intensity $(V/m)^4$) and theoretical field intensity models (in $(V/m)^2$) of monomers/dimers, predicting the enhancement effect upon coupling.

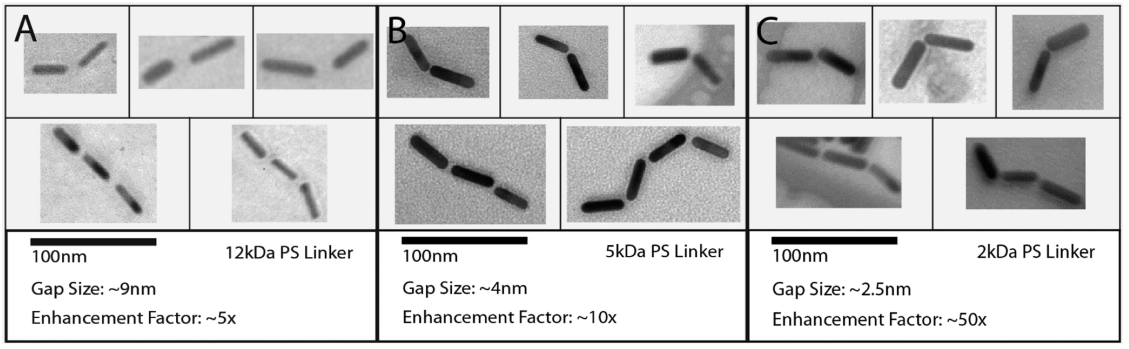

Figure 5. TEM comparison images of encapsulated nanorod chains utilizing polystyrene linkers of varying MW: 12 kDa (A), 5 kDa (B), and 2 kDa (C), showing the reduction in gap size and increase in observed enhancement as polymer MW decreases.

previous work[26] to collected UV–vis–NIR spectra) aqueous solution of encapsulated NR aggregates was examined *via* Raman spectroscopy to evaluate the enhancement of the SERS signal (Figure 4). For comparison, the spectrum of NR monomers is plotted on the same graph. When considering the 563 and 604 cm^{-1} vibrational modes of the phenoxazine rings of the Raman probe,[27] an ~9× enhancement of the Raman signal was observed for the solution of lipid-encapsulated NR aggregates as compared to the NR monomers. These unassembled monomers, which incorporated the Raman probe in the end region (functionalized with 5 kDa PS and possessing an ~4 nm inter-rod gap), themselves showed an enhancement of ~15× over a solution of the probe without NRs (Figure 4A). The 5 kDa PS was chosen to test if a shorter inter-rod gap would be reliably observed (compared to 12 kDa PS) prior to attempting the use of PS of even lower MW. The stable enhancement was attributed to controlled NR aggregation. A total of six trials were done to test for reproducibility. Raman signal peak intensity varied by a factor of 0.8–1.3 among the trials. The standard deviation was 12% (Figure 4A, Supporting Information). In addition, the system was tested with two alternate Raman markers, and signals from the markers were observed (Supporting Information). The gap size between the NR ends controlled the observed SERS enhancement due to increased electric field intensity in the measured inter-rod gap, with shorter gap sizes dramatically increasing observed enhancement, as shown in Figure 4B and Figure 5.

As expected, with shorter 2 kDa polystyrene, a significant increase in enhancement (46–50× with an approximate 2.5 nm gap size) was observed. The enhancement results observed with varying linkers (and thus varying inter-rod gap sizes) are displayed in Figure 5.

CONCLUSIONS

We report an approach to the generation of functional gold NR aggregates that provide strong Raman intensities useful for temporally stable, bright plasmonic biosensors in solution state. We halted the aggregation of gold NRs *via* phospholipid encapsulation and achieved an increase of ~50× in the Raman signal of the Oxazine 725 reporter, as compared to that of NR monomers (and ~750× over bare dye). We demonstrated a progression of enhancement as polystyrene molecular weight and gap size decrease.

Most importantly, we have demonstrated a method that balanced the self-assembly of polymer-functionalized nanorods and the creation of narrow inter-rod gaps. This method achieved selective isolation of short nanorod chains that display maximized relative enhancement, which has not previously been reported. We believe that the developed lipid-encapsulated NR-based SERS probes will allow for increased probe customizability as a result of potential functionalization of the lipid environment.[20] The approach reported here offers several potential advantages over spherical NP aggregates. First, the scattered light is in the near-infrared "window" region for water and tissues.[21] Second, there are stronger fields between NR ends than between nanospheres, and hence greater scattering efficiency per unit area. The approach could be extended to rods of different sizes and aspect ratios, and aggregates of differing gaps, to enable function at other wavelengths. Finally, when creating multifunctional NPs including therapeutic NPs, the NR aggregate approach could be used in photothermal therapy.[28]

MATERIALS AND METHODS

Synthesis and Functionalization of Gold Nanorods. Nanorod synthesis was carried out in the fashion described by El-Sayed.[23] A 4.5 g portion of cetyltrimethylammonium bromide (CTAB), purchased from Sigma-Aldrich, was placed in a 125 mL Erlenmeyer flask, along with 50 g of water. This flask was heated in a warm water bath until the CTAB dissolved. A 3.38 g amount of a 4 mM $AgNO_3$ solution was added while shaking. Then 5.6 g of a 12.5 mM $AuCl_3$ solution was added while shaking. Another 45 g of water (resulting in ~100 mL of solution) was then added, resulting in a red-orange solution. This solution was then stored at 27 °C. A 210 mg amount of L-ascorbic acid and 15 g of water were placed into a scintillation vial. This was agitated until the acid dissolved. This solution was added to the above dropwise (with drops counted) until the solution was observed to turn clear. An additional number of drops corresponding to 25% of those already added were then added, to ensure sufficient acid addition. The combined solution was again stored at 27 °C. A 200 mg sample of CTAB and 3.5 g of water were placed into a scintillation vial. These were heated in a warm water bath until the CTAB dissolved, and a stirring bar was added. Then 150 μL of the 12.5 mM $AuCl_3$ solution was added, resulting in a yellow solution.

Into a scintillation vial were placed 5.7 mg of $NaBH_4$ and 15 g of water. This was placed in an ice bath to cool. While stirring at high speed, 500 μL of the $NaBH_4$ solution was added to the previous solution-containing vial. This was allowed to stir for 30 s and then removed to sit for 5 min. The solution was observed to change to a brown color over this period. After 5 min, 1000 μL of the previous solution was added to the initial solution. This was capped and stored overnight at 27 °C, changing to a deep purple color as the nanorods formed. Approximately 60 1.5 mL Eppendorf vials were filled with the raw solution of CTAB-stabilized nanorods described above. Excess CTAB was removed *via* centrifugation at 7675 rcf for 30 min (removing the supernatant and keeping the deposited nanorods). The concentrated nanorods were then sonicated with 6 mg of 5 kDa polystyrene (purchased from Polymer Source Inc.) in 10 g of THF for 30 min. This solution was left overnight, and excess polystyrene was removed *via* eight cycles of centrifugation at 7675 rcf for 30 min, with supernatant removal and replacement between each cycle.

Following the final cycle, all concentrated nanorod solutions were combined and diluted up to a volume in 10 g of THF. Equivalent amounts of 12/5/2 kDa PS were introduced for their trials. A 300 μL amount of the previous polystyrene-functionalized nanorods in THF was placed into a scintillation vial. The THF was evaporated under air. A 2 mL portion of a 20 μM solution of Oxazine 725 in DMF was then added. This was allowed to equilibrate for 30 min prior to use.

Preparation of Phospholipid Solution. The lipid mixture utilized was DEC221, a 2:2:1 proportional mole ratio mixture of a 1,2-dioleoyl-*sn*-glycero-3-phosphocholine (DOPC) solution in chloroform (provided at 100 mg of DOPC in 4 mL of chloroform), solid egg sphengomyelin (ESM), and solid bovine cholesterol, all purchased from Avanti Polar Lipids. A 1.1 mL sample of the DOPC solution (equivalent to 0.035 mmol) was utilized as a base, and to this were added 0.035 mmol of ESM and 0.0175 mmol of cholesterol, resulting in approximately 60 mg of lipid mixture in solution in a 2:2:1 mol ratio. This lipid mixture was divided into 1 dram vials in a proportion of 3 mg of lipids/vial, desiccated overnight, and placed in a freezer for storage. The dried solutions were rehydrated with 1 mL of water and heated at 50 °C for 30 min, producing a turbid suspension of large multilamellar vesicles. Following this, the solution was repeatedly passed through an extruder utilizing a 30 nm filter for a total of eight passes to produce small unilamellar vesicles (ULVs). The ULV solution was then diluted with water to a total volume of 2.5 mL and placed aside for use.

Self-Assembly Initiation/Termination and Characterization. Self-assembly was initiated *via* dropwise addition of 500 μL of water to the 2 mL solution of Oxazine 725-associated nanorods. Self-assembly was terminated *via* dropwise addition of the self-assembling solution to the aqueous solution of ULVs. Confirmation of SA quenching was obtained via UV–vis–NIR spectroscopy collected on a Cary 5000 spectrophotometer, which was also utilized for all subsequent UV–vis–NIR spectrometry. The organic/aqueous (DMF/water) solvent system containing the encapsulated solution was placed in dialysis tubing and subjected to dialysis with an aqueous medium for a period of 24 h. The resultant solution was then investigated *via* Raman spectroscopy to confirm the removal of the organic portion of the matrix (below). Raman characterization was performed on a NuSpec Advantage Raman spectrometer with a 785 nm laser. Population analysis of the nanorod aggregation numbers was accomplished through the collection of a number of TEM images at representative stages of the assembly process (30 min, 1 h, after solvent exchange, *etc.*). Approximately 600 individual nanorods from each assembly stage were examined and categorized by species (monomer, dimer, trimer, *etc.*). These examinations were repeated for each assembly utilizing polystyrene of differing MW. Histograms of the numbers of nanorods aggregated in chains at different stages of assembly were prepared. Nanorod aspect ratio data and gap size measurements were made by importing collected images into ImageJ, followed by use of the program's measurement function, using the scale bar provided by the TEM images as a reference (Supporting Information). TEM images were collected using a Hitachi H-7000 microscope operating at 75 kV.

Enhancement Comparison Method. To obtain the normalized relative signal as reported, the collected Raman spectra were normalized relative to a collected spectrum of pure DMF (present in equal amounts at the initiation of assembly). The signal from the encapsulated, aqueous nanorod solution was then scaled by a factor equal to that of the observed drop in solution (and hence nanorod) concentration (based on collected peak heights) between a preassembly state and the final encapsulated, aqueous state, as determined from UV–vis–NIR spectra of the assembly profile. A decreasing trend was observed in collected Raman spectra of a self-assembling solution as time progressed (and proportions of longer-chain species increased), indicating the desirability of short-chain species for maximum observed enhancement.

Theoretical Field Modeling. Theoretical modeling was performed through finite-difference time-domain (FDTD) to investigate the separation-dependent coupling effects in end-to-end assembled NRs.

Conflict of Interest: The authors declare no competing financial interest.

Acknowledgment. The authors thank I. Gourevich and N. Coombs of the Centre for Nanostructure Imaging for assistance in acquiring TEM and other images. This work was supported by the NSERC Strategic Network for Bioplasmonic Systems (Biopsys). The authors would also like to thank R. Gordon, of the University of Victoria, for access to the modeling software used for theoretical FDTD simulations.

Supporting Information Available: Raman spectra analyzing solvent exchange and utilizing different linkers. Measurement of Raman signal from lipid and additional Raman probes. Reproducibility data. Complete theoretical models. This material is available free of charge *via* the Internet at http://pubs.acs.org.

REFERENCES AND NOTES

1. Glotzer, S. C.; Solomon, M. Anisotropy of Building Blocks and Their Assembly into Complex Structures. *Nat. Mater.* **2007**, *6*, 557–562.
2. Bedford, E.; Spadavecchia, J.; Pradier, C.; Gu, F. X. Surface Plasmon Resonance Biosensors Incorporating Gold Nanoparticles. *Macromol. Biosci.* **2012**, *12*, 724–739.
3. Mayer, K. M.; Hafner, J. H. Localized Surface Plasmon Resonance Sensors. *Chem. Rev.* **2011**, *111*, 3828–3857.
4. Liu, N.; Mukherjee, S.; Bao, K.; Li, Y.; Brown, L. V.; Nordlander, P.; Halas, N. J. Manipulating Magnetic Plasmon Propagation in Metallic Nanocluster Networks. *ACS Nano* **2012**, *6*, 5482–5488.
5. Stewart, M. E.; Anderton, C. R.; Thompson, L. B.; Maria, J.; Gray, S. K.; Rogers, J. A.; Nuzzo, R. G. Nanostructured Plasmonic Sensors. *Chem. Rev.* **2008**, *108*, 494–521.
6. Wang, Y. Q.; Yan, B.; Chen, L. X. SERS Tags: Novel Optical Nanoprobes for Bioanalysis. *Chem. Rev.* **2013**, *113*, 1391–1428.
7. Nabika, H.; Oikawa, T.; Iwasaki, K.; Murakoshi, K.; Unoura, K. Dynamics of Gold Nanoparticle Assembly and Disassembly Induced by pH Oscillations. *J. Phys. Chem. C* **2012**, *116*, 6153–6158.
8. Durand-Gasselin, C.; Sanson, N.; Lequeux, N. Reversible Controlled Assembly of Thermosensitive Polymer-Coated Gold Nanoparticles. *Langmuir* **2012**, *27*, 12329–12335.
9. Sanchez-Iglesias, A.; Grzelczak, M.; Altantzis, T.; Goris, B.; Perez-Juste, J.; Bals, S.; Van Tendeloo, G.; Donaldson, S. H.; Chmelka, B. F.; Israelachvili, J. N.; *et al.* Hydrophobic Interactions Modulate Self-Assembly of Nanoparticles. *ACS Nano* **2012**, *6*, 11059–11065.
10. Lukach, A.; Liu, K.; Therien-Aubin, H.; Kumacheva, E. Controlling the Degree of Polymerization, Bond Lengths, and Bond Angles of Plasmonic Polymers. *J. Am. Chem. Soc.* **2012**, *134*, 18853–18859.
11. Tabor, C.; Van Haute, D.; El-Sayed, M. A. Effect of Orientation on Plasmonic Coupling between Gold Nanorods. *ACS Nano* **2009**, *3*, 3670–3678.
12. Chen, G.; Wang, Y.; Tan, L. H.; Yang, M.; Tan, L. S.; Chen, Y.; Chen, H. High-Purity Separation of Gold Nanoparticle Dimers and Trimers. *J. Am. Chem. Soc.* **2009**, *131*, 4218–4219.
13. Lee, A.; Andrade, G. F. S.; Ahmed, A.; Souza, M. L.; Coombs, N.; Tumarkin, E.; Liu, K.; Gordon, R.; Brolo, A. G.; Kumacheva, E. Probing Dynamic Generation of Hot-Spots in Self-Assembled Chains of Gold Nanorods by Surface-Enhanced Raman Scattering. *J. Am. Chem. Soc.* **2011**, *133*, 7563–7570.
14. Grzelczak, M.; Mezzasalma, S. A.; Ni, W.; Herasimenka, Y.; Feruglio, T. M.; Perez-Juste, J.; Fornasiero, P.; Prato, M.; Liz-Marzan, L. M. Antibonding Plasmon Models in Colloidal Gold Nanorod Clusters. *Langmuir* **2012**, *28*, 8826–8833.
15. Gómez-Graña, S.; Pérez-Juste, J.; Alvarez-Puebla, R. A.; Guerrero-Martínez, A.; Liz-Marzán, L. M. Self-Assembly of Au@Ag Nanorods Mediated by Gemini Surfactants for Highly Efficient SERS-Active Supercrystals. *Adv. Optical Mater.* **2013**, *1*, 477–481.
16. Gómez-Graña, S.; Goris, B.; Altantzia, T.; Fernández-López, C.; Carbó-Argibay; Guerrero-Martínez, A.; Almore-Barrios, N.; López, N.; Pastoriza-Santoz, I.; Pérez-Juste, J.; *et al.* Au@Ag Nanoparticles: Halides Stabilize {100} Facets. *J. Phys. Chem. Lett.* **2013**, *4*, 2209–2216.
17. Osberg, K.; Rycenga, M.; Harris, N.; Schmucker, A. L.; Langrille, M. R.; Schatz, G. C.; Mirkin, C. A. Dispersible Gold Nanorod Dimers with Sub-5nm Gaps as Local Amplifiers for Surface-Enhanced Raman Scattering. *Nano Lett.* **2012**, *12*, 3828–3832.
18. Huff, T. B.; Hansen, M. N.; Zhao, Y.; Cheng, J. X.; Wei, A. Controlling the Cellular Uptake of Gold Nanorods. *Langmuir* **2007**, *23*, 1596–1599.
19. Tam, N. C. M.; McVeigh, P. Z.; MacDonald, T. D.; Farhadi, A.; Wilson, B. C.; Zheng, G. Porphyrin-Lipid Stabilized Gold Nanoparticles for Surface Enhanced Raman Scattering Based Imaging. *Bioconjugate Chem.* **2012**, *23*, 1726–1730.
20. Tam, N. C. M.; Scott, B. M. T.; Voicu, D.; Wilson, B. C.; Zheng, G. Facile Synthesis of Raman Active Phospholipid Gold Nanoparticles. *Bioconjugate Chem.* **2010**, *21*, 2178–2182.
21. Ip, S.; MacLaughlin, C. M.; Gunari, N.; Walker, G. C. Phospholipid Membrane Encapsulation of Nanoparticles for Surface-Enhanced Raman Scattering. *Langmuir* **2011**, *27*, 7024–7033.
22. Ip, S.; MacLaughlin, C. M.; Mullaithilaga, N.; Joseph, M.; Wala, S.; Wang, C.; Walker, G. C. In Lipid-Encapsulation of Surface Enhanced Raman Scattering (SERS) Nanoparticles and Targeting to Chronic Lymphocytic Leukemia (CLL) Cells, *Proc. SPIE* 8212, Frontiers in Biological Detection: From Nanosensors to Systems IV, 821204 (February 9, **2012**); doi:10.1117/12.909179.
23. Nikoobakht, B.; El-Sayed, M. A. Preparation and Growth Mechanism of Gold Nanorods (NRs) Using Seed-Mediated Growth Method. *Chem. Mater.* **2003**, *15*, 1957–1962.
24. Nie, Z.; Fava, D.; Kumacheva, E.; Zou, S.; Walker, G. C.; Rubinstein, M. Self-Assembly of Metal-Polymer Analogues of Amphiphilic Triblock Copolymers. *Nat. Mater.* **2007**, *6*, 609–614.
25. Liu, K.; Resetco, C.; Kumacheva, E. Salt-Mediated Kinetics of the Self-Assembly of Gold Nanorods End-Tethered with Polymer Ligands. *Nanoscale* **2012**, *4*, 6574–6580.
26. Orendorff, C. J.; Murphy, C. J. Quantitation of Metal Content in the Silver-Assisted Growth of Gold Nanorods. *J. Phys. Chem. B* **2006**, *110*, 3990–3994.
27. Brolo, A. G.; Sanderson, A. C.; Smith, A. P. Ratio of the Surface-Enhanced Anti-Stokes Scattering to the Surface-Enhanced Stokes-Raman Scattering for Molecules Adsorbed on a Silver Electrode. *Phys. Rev.* **2004**, *69*, 045424.
28. Huang, X. H.; Neretina, S.; El-Sayed, M. A. Gold Nanorods: From Synthesis and Properties to Biological and Biomedical Applications. *Adv. Mater.* **2009**, *21*, 4880–4910.